Effects of longitudinal disturbances on two-dimensional detonation waves

Xuechen Xi [1], Honghui Teng [1,*], Zheng Chen [2], and Pengfei Yang [2,†]

[1]*Department of Mechanics, School of Aerospace Engineering, Beijing Institute of Technology, Beijing 100081, China*

[2]*SKLTCS, CAPT, College of Engineering, Peking University, Beijing 100871, China*

Gaseous cellular detonation is unsteady, and its propagation dynamics in a uniform mixture have been widely studied, but there are few works on cellular detonations in continuously disturbed media. Based on two fundamental propagation modes: stable (with regular cells) or unstable (with irregular cells), this study uses the Euler equations coupled with a two-step chemical reaction model to investigate two-dimensional cellular detonations with longitudinal disturbances. Disturbed detonations are generated by introducing a longitudinal sinusoidal density disturbance whose bifurcation parameter is the disturbance wavelength λ. The detonation cell distributions and propagation features are analyzed by recording the maximum local pressure and presenting the frequency spectrum of the averaged cell pressure. It is observed that the ratio of longitudinal disturbance wavelength λ to reaction zone width W_R plays an important role in cell morphology. For regular detonations, the cell scale changes periodically with the disturbance cycle, and the fundamental frequency of the averaged pressure signals is consistent with the disturbance frequency when this ratio is much greater than 1. If the ratio has a single-digit value, the original coupling relationship of shock waves and reaction fronts is destroyed and rebuilt, leading to an intermittent and local detonation decoupling and reinitiation. The size of newly formed large cells reaches about 3–6 times the size of the undisturbed cell. However, there are different cell-size spectra for stable and unstable detonations attributed to different transverse wave regularities. By introducing acoustic impedance analyses, the interaction of the detonation wave and varying density interface is presented, and the role of a sinusoidal density disturbance in wave dynamics is discussed.

I. INTRODUCTION

Gaseous detonation can be considered a leading shock wave followed by a heat-release zone, meaning that gain-pressure combustion could be obtained via a detonation mode [1–3]. Due to the high thermal efficiency of detonation combustion, the concept of propulsion systems based on detonations has attracted increasing attention, prompting important progress in detonation engines [4–7]. In particular, hypersonic air-breathing configurations offer the potential for fast long-distance civil transport [8]. But, detonation combustion differs markedly from diffusive combustion, which is mainly dependent on heat and species transport. A premixed and homogeneous mixture is perfect for detonation waves, but this is not realistic in industrial applications. Incomplete mixing and an inhomogeneous medium would be an intrinsic feature of any realistic air-breathing propulsor [9–12].

---

*hhteng@bit.edu.cn

†young1505@foxmail.com

A gaseous detonation wave is inherently unsteady and involves strong shock interface instabilities [13] and combustion instabilities [14], leading to multidimensional cellular structures [15,16]. Extrinsic disturbances, such as density, temperature, and velocity gradients, could couple with the inherent instabilities of a detonation wave, which is a significant challenge in disturbed detonation research.

In a preliminary study, Ishii and Kojima [17] experimentally studied the behavior of detonation waves in a mixture with concentration gradients normal to the propagation direction. They found that an increase in concentration gradient can deflect the angle of the detonation front. For a low activation energy mixture, detonations could survive in the nonuniform cases considered, and the velocity approached the Chapman-Jouguet (CJ) velocity for the stoichiometric mixture [18]. However, complete quenching and a speed deficit were observed for the high activation energy mixture with a larger concentration gradient. A 9% maximum velocity deficit compared with the CJ velocity was also observed in the experiments, and the steep transverse concentration gradients at low average hydrogen concentrations resulted in a single-headed detonation [19]. Given the longitudinal equivalence ratio distributions parallel to the detonation propagation direction, experimental investigations on the dynamic behavior of detonations in nonuniform mixtures have been reported [20,21]. These studies concluded that the detonation quenching mechanisms appear to be controlled by the composition variation rate and detonation characteristic lengths.

A discontinuous interface and spatially inhomogeneous thermodynamic properties may occur in detonable media for incomplete mixing and slot injection in detonation engines. Tang-Yuk et al. [22] investigated the wave patterns of a detonation wave theoretically and numerically by introducing a density interface into the mixture. They found that an interface density decrease causes a decreased leading shock pressure, meaning that the transmitted wave is weaker than the incident detonation wave. In extreme cases, a detonation wave enters an inert layer in which a transient decoupling phenomenon occurs because of a lack of reactants. The ratio of the inert layer thickness to the intrinsic induction length of a Zel'dovich–von Neumann–Döring (ZND) detonation wave dominates the detonation wave dynamics [23]. Above a critical value, the quench phenomenon of a detonation wave across the inert layer could be observed. Wang et al. [24] presented a study of a stoichiometric hydrogen-oxygen-nitrogen mixture with multiple inert layers. Results revealed a critical inert layer thickness above which the detonation wave fails after crossing the inert layers for a given inert layer spacing.

In contrast to the studies mentioned above that mainly focused on entire inert layers, Mi et al. [25,26] introduced spatially discretized energy sources into the combustible medium, where a discrete burning source can drive a blast wave supporting the detonation front. In their studies, the detonation velocity of the mixture with highly discretized energy sources was greater than the CJ velocity of a homogeneous medium with the same energy release. This super-CJ wave can be interpreted as a weak detonation for which the generalized CJ condition applies at a nonequilibrium state, and the sonic point occurs before the end of the heat-release zone [26].

Because of the effects of species diffusion and convective transport, the thermodynamic and chemical properties before the detonation wave vary almost continuously in space for realistic experiment conditions [27,28]. The dynamic behavior of one detonation wave in a continuous and long-distance disturbed mixture is important to applications of detonation waves in engines. As a first step to elucidate the nonlinear modes of pulsating detonations, recent studies [29,30] introduced a periodic longitudinal disturbance to a mixture, and the responses of one-dimensional detonation waves were reported. The results have shown that the disturbance frequency and amplitude can change the detonation propagation modes [29]. The interactions between intrinsic instability and small perturbations could cause the regularization of chaotic detonation oscillations [30].

Mode locking of detonation dynamics has also been observed [31], and the upstream-state variation imposes the detonation wave oscillation mode. However, the gaseous detonation wave has a transient and multidimensional structure involving leading shock and transverse wave interactions. The cellular detonation's response in a nonuniform mixture with a continuously spatial variation is

still unclear. It remains to be resolved whether the upstream variation can impose multidimensional cells.

The present study considers two-dimensional cellular detonation propagation in inhomogeneous mixtures with sinusoidal density distributions parallel to the propagation direction. The cell patterns and cell-size spectra of two fundamental propagation modes—stable (with regular cells) or unstable (with irregular cells)—are presented to examine longitudinal disturbance effects. The average pressure and velocity of the disturbed detonation and their distributions are also measured. Interactions of the density disturbance on the detonation front are discussed to examine whether mode-locking detonation dynamics can occur in two-dimensional cellular detonations.

II. SIMULATION DETAILS

A. Governing equations and reaction model

For a detonation wave in a wide channel, the viscosity effects are composed of two parts: viscous diffusion and a wall-induced boundary layer. Diffusion can suppress the small-scale vortices at shear layers, and the low-energy near-wall flow interacts with shock structures, meaning that large-scaled shock structures obtained by solving the Euler and Navier-Stokes equations are qualitatively similar for irregular detonations [32]. For highly irregular detonations, small-scale wave structures in detonation products, such as unburned gas pockets, may be affected by diffusion, but little is known about the underlying mechanisms. This work focuses on the disturbance regulation effect on large-scaled shock structures and propagation dynamics. Hence, the compressional Euler equations are employed with the two-step induction-reaction model for H_2 and air to simulate two-dimensional detonation waves. The governing equations are expressed as

$$\frac{\partial \rho}{\partial t} + \frac{\partial (\rho u)}{\partial x} + \frac{\partial (\rho v)}{\partial y} = 0, \tag{1}$$

$$\frac{\partial (\rho u)}{\partial t} + \frac{\partial (\rho u^2 + p)}{\partial x} + \frac{\partial (\rho uv)}{\partial y} = 0, \tag{2}$$

$$\frac{\partial (\rho v)}{\partial t} + \frac{\partial (\rho uv)}{\partial x} + \frac{\partial (\rho v^2 + p)}{\partial y} = 0, \tag{3}$$

$$\frac{\partial \rho e}{\partial t} + \frac{\partial [\rho u(e + p)]}{\partial x} + \frac{\partial [\rho v(e + p)]}{\partial y} = 0, \tag{4}$$

where e is the specific total energy considering chemical energy heat release, given by

$$e = \frac{p}{\rho(\gamma - 1)} + \frac{u^2 + v^2}{2} - \eta Q, \tag{5}$$

and the ideal gas equation of state can be expressed as

$$T = \frac{p}{\rho}, \tag{6}$$

where u, v, p, ρ, and T are the x- and y-direction velocities, pressure, density, and temperature, respectively. All variables are scaled by reference to the uniform unburned state as follows (the tilde, $\sim$, denotes the original dimensional quantities and the subscript 0 indicates the reference quantities upstream of the detonation (shock-) front:

$$\rho = \frac{\tilde{\rho}}{\rho_0}, \quad p = \frac{\tilde{p}}{p_0}, \quad T = \frac{\tilde{T}}{T_0}, \quad u = \frac{\tilde{u}}{\sqrt{RT_0}}, \quad Q = \frac{\tilde{Q}}{RT_0}. \tag{7}$$

The current work focuses on the detonation dynamics in a nonuniform mixture. A long channel (about 5000 times longer than the induction zone length) is required to obtain a quasisteady

detonation wave. The extremely high computational cost must be considered, especially for two-dimensional cellular detonations. Therefore, a two-step reaction model is considered. For the two-step chemistry, the chemical reaction of the combustible mixture is decomposed into two steps. The first step describes the mixture ignition decay. The second step is the heat release corresponding to the chain combination. The two stages can be characterized by the Arrhenius reaction law and can be expressed by [33]

$$\frac{\partial(\rho\xi)}{\partial t} + \frac{\partial(\rho u\xi)}{\partial x} + \frac{\partial(\rho v\xi)}{\partial y} = H(1-\xi)\rho k_I \exp\left[E_I\left(\frac{1}{T_S} - \frac{1}{T}\right)\right], \tag{8}$$

$$\frac{\partial(\rho\eta)}{\partial t} + \frac{\partial(\rho u\eta)}{\partial x} + \frac{\partial(\rho v\eta)}{\partial y} = [1 - H(1-\xi)]\rho(1-\eta)k_R \exp\left[-\frac{E_R}{T}\right], \tag{9}$$

where ξ and η represent the progress variables for the induction and heat-release zones, respectively; $H(1–\xi)$ is a Heaviside step function (1 when $\xi \leqslant 1$ or 0 if $\xi > 1$).

This two-step model employs the constant specific-heat ratio (γ) approximation with a constant heat release Q. The main model parameters are the activation energies E_I and E_R, and the preexponential factors k_I and k_R. T_S is the von Neumann temperature behind the leading shock front of a one-dimensional detonation with a ZND structure. T_S is 2.429 for $T_0 = 500$ K, and 3.074 for $T_0 = 700$ K. Following a previous study [33], the induction length of the one-dimensional ZND detonation is normalized and fixed to unity. Hence, the factor k_I is set to $-u_{vn}$, where u_{vn} is the particle velocity behind the leading shock in the shock-fixed frame of the one-dimensional ZND detonation. For the simulation of H$_2$-air detonation combustion, the other chemical parameters are obtained by referring to the detailed reaction mechanism.

In modeling the detonation in a given H$_2$-air mixture with a specified pressure, temperature, and species, the unknown chemical parameters to be determined are primarily the heat release Q, specific-heat ratio γ, activation energies E_I and E_R, and preexponential factor k_R. In the modeling, V_{CJ}, M_{CJ}, and a combined instability parameter χ are required for consistency with the detailed H$_2$-air mechanism [34]. The Mach number M_{CJ} of a detonation wave is given by

$$M_{CJ} = \left[\left(1 + \frac{\gamma^2-1}{\gamma}Q\right) + \sqrt{\left[\left(1 + \frac{\gamma^2-1}{\gamma}Q\right)^2 - 1\right]}\right]^{1/2}, \tag{10}$$

where M_{CJ} is defined as

$$M_{CJ} = \frac{V_{CJ}}{\sqrt{\gamma R T_0}}. \tag{11}$$

The specific-heat ratio γ of the two-step model is assumed to be consistent with the von Neumann state of a detonation wave [35]. The stability parameter χ is defined as

$$\chi = \varepsilon_I \frac{\Delta_I}{\Delta_R}, \tag{12}$$

where Δ_I and Δ_R denote the induction length and reaction length of a one-dimensional (1D) ZND detonation, respectively [33], and ε_I is the ratio of E_I to T_S. By solving for the 1D ZND detonation structure, the main chemical parameters of the two-step model can be determined efficiently [34].

Notably, to investigate the dynamics of a cellular detonation wave in a disturbed medium, two typical detonations displaying stable and unstable modes are considered in this study. For an H$_2$-air detonation wave at a standard atmospheric temperature of 300 K, the cells are highly irregular and difficult to distinguish clearly in disturbed media. Hence, the mixture temperature is increased to 700 and 500 K to obtain stable and middle-unstable detonations, respectively. The main chemical parameters in this two-step model are listed in Table I, in which the temperature varies, but the pressure is fixed at 1 atm. All variables have been scaled by reference to the uniform unburned state. The details of the dimensionless method can be found in previous studies [34,35].

TABLE I. Two-step model parameters of stoichiometric H_2-air mixtures.

	Stable	Unstable
T (K)	700	500
Q	7.189	10.761
γ	1.309	1.313
E_I	$5.72T_S$	$6.20T_S$
E_R	$0.7T_S$	$0.7T_S$
k_R	1.515	2.371
χ	1.378	2.389

B. Numerical approaches

A schematic of a two-dimensional (2D) detonation wave propagating in a nonuniform mixture having a sinusoidal density distribution is shown in Fig. 1. First, a cellular detonation wave in a uniform mixture is simulated; then, the mixture ahead of the detonation front is subjected to a continuous density disturbance. To avoid the interference of pressure-driven flow in the unburned mixture, we keep the mixture pressure constant and disturb only the density and temperature with a sinusoidal function. The density distribution is related to the spatial position and is given by $\rho = \rho_0 + A\sin[(2\pi/\lambda)x]$, where ρ_0 is the density of the uniform mixture, i.e., $\rho_0 = 1.0$. The disturbance amplitude A is chosen to be 10% of the initial density in this study, i.e., $A = 0.1\rho_0$. The disturbance wavelength λ can be adjusted to mimic the nonuniformity of the reactant. When λ is infinite, the density ρ is a constant value ρ_0, and the mixture is uniform.

The governing equations are solved using the advection upstream splitting method with a third-order monotone upstream-centered scheme for conservation laws (MUSCL) approach [36]. The third-order Runge-Kutta algorithm is chosen as the time-discretization scheme to provide high-resolution simulations. The slip-boundary condition, modeled as mirror symmetry, is used on the top and bottom walls. The left and right boundaries are open to the ambient conditions.

The width of the channel is $H = 240\Delta_I$. Notably, the propagation of a cellular detonation in a disturbed medium requires a large computational domain. The computational cost is reduced by employing an "adjustable domain," and the switching process schematics are illustrated in Fig. 2. During the simulation, a detonation wave propagates from left to right in the channel (L_n). When the detonation front reaches the switching point in the computation domain, the code extends the computational domain to the right, and the left domain is simultaneously truncated.
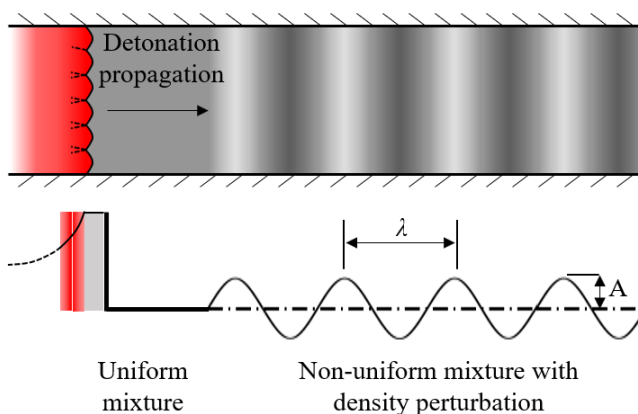

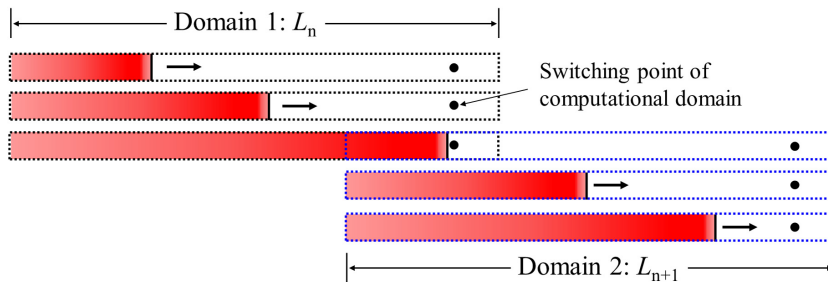FIG. 1. Schematic of a two-dimensional detonation wave in a disturbed medium.

FIG. 2. Switching of the adjustable computational domain.

Then, a new domain (L_{n+1}) forms, allowing the detonation front to propagate continuously. The computational domain is continuously updated in the calculations to obtain a quasisteady detonation in the disturbed medium. The left exit is located far from the detonation front and open to the ambient to avoid truncation effects. The length of the computational domain is related to disturbance wavelength λ but is always greater than $200\Delta_I$. If λ is greater than $200\Delta_I$, the length L equals λ. If λ is less than $200\Delta_I$, the length L can be obtained from the formulas $L = m \times \lambda$ ($m = 2, 3, 4 \ldots$). The coefficient m should satisfy the criteria $m \times \lambda > 200\Delta_I$ and $(m-1) \times \lambda < 200\Delta_I$.

III. UNDISTURBED CASES AND GRID RESOLUTION STUDY

The 2D cellular detonation wave in a uniform mixture is simulated first, and the related detonation front structures and numerical cells are shown in Figs. 3 and 4. The numerical cells are presented by recording the maximum local pressure. A typical stable mode-detonation wave pattern is shown in Fig. 3. The wave structures on the detonation surface are clear and easily distinguished. A decrease in the mixture temperature from 700 to 500 K results in a higher χ, which leads to a more unstable detonation wave. The related cells become more irregular, and the size of numerical cells change around a specified value, as shown in Fig. 4(c).

This study defines N_i as the number of grid points per induction length of a one-dimensional ZND detonation. To illustrate grid convergence, Fig. 5 shows numerically computed cells for $N_i = 10$,
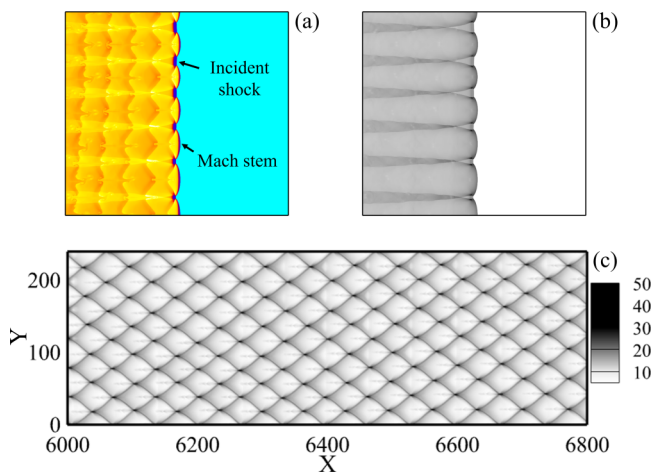
FIG. 3. Stable detonation ($T = 700$ K, $P = 1$ atm) propagation in a uniform medium: (a) temperature contours; (b) pressure contours; (c) numerical cells.
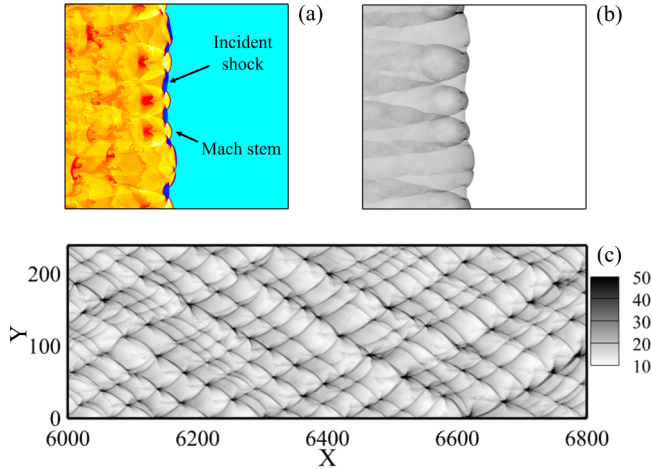
FIG. 4. Unstable detonation ($T = 500$ K, $P = 1$ atm) propagation in a uniform medium: (a) temperature contours; (b) pressure contours; (c) numerical cells.

20, and 40. Note that all the length variables have been scaled by the induction length and are dimensionless in this study.

For the stable detonation shown in Figs. 5(a)–5(c), the cells are regular at different grid scales, and the cell size is approximately equal to 40.6. For the unstable detonations, the cell sizes are distributed over a range, so the characteristic size of detonation cells is represented by the average value. For the grid scales $N_i = 10$, 20, and 40, the average cell sizes are 38.5, 41.5, and 42.2, respectively. Following the standard methodologies described in the literature [37,38], the fine-grid convergence index (GCI) is a function of the approximate relative error for two grid scales. For the results of Figs. 5(a)–5(c), the GCIs of the cell sizes are 2.7 and 0.6%, respectively. Therefore, the numerical uncertainty in the fine-grid solution for the cell size is 0.6%. The average apparent order of accuracy, i.e., p_{ave}, is 2.16, which is a good indication of the third-order MUSCL approach applied for this calculation. The cell patterns and cell sizes for different grid scales are qualitatively consistent.

In addition to the accuracy estimates of the simulated cell sizes, the cell-pressure values are also important to the simulation objectives. The pressure profiles along the cell centerline, the related
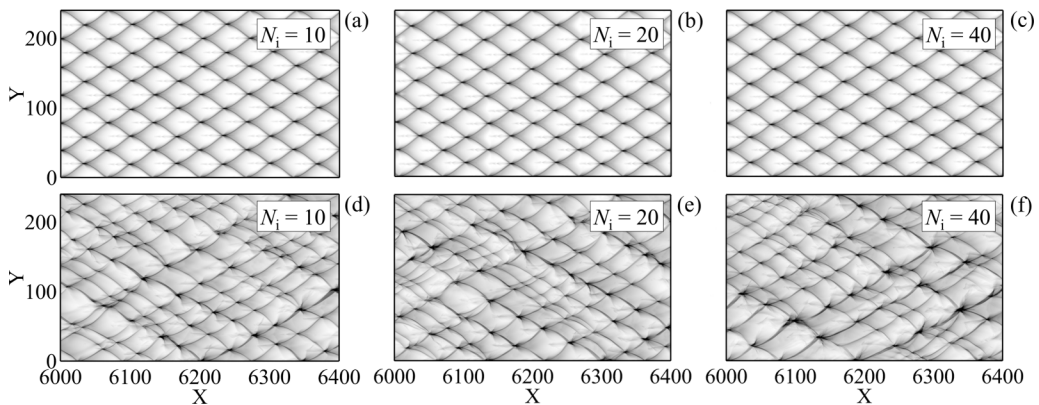

FIG. 5. Numerical detonation cells at different grid resolutions at an initial temperature of (a)–(c) $T = 700$ K, and (d)–(f) $T = 500$ K.
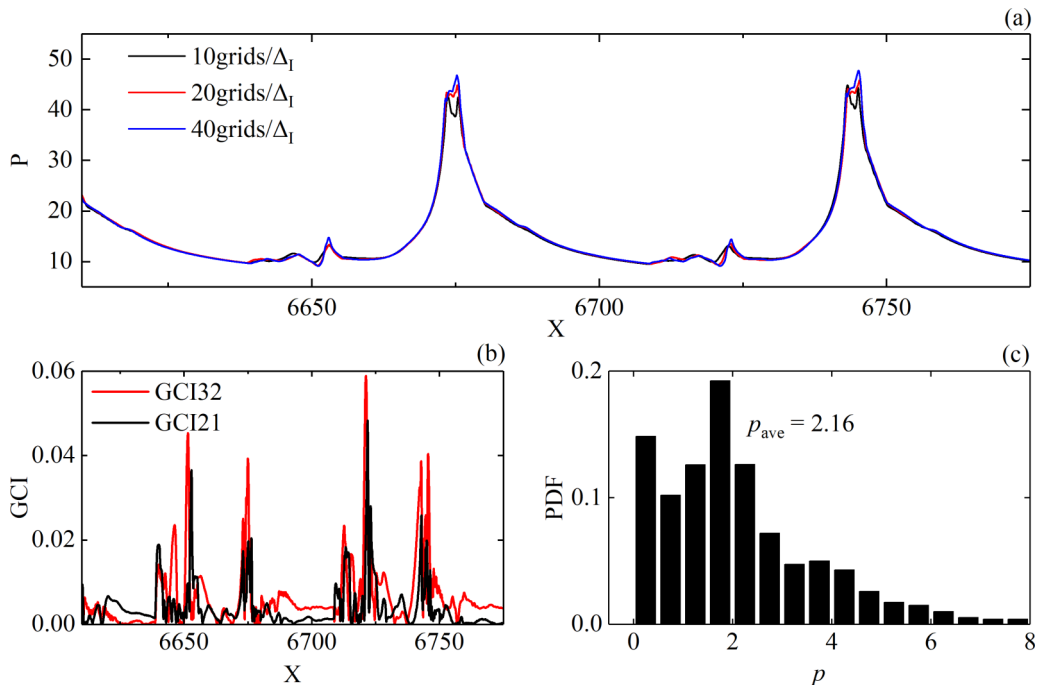
FIG. 6. Pressure profiles along the centerline of the numerical cell for different grids: (a) GCIs distributions; (b) GCI32 denotes the results for $N_i = 10$ and 20, and GCI21 denotes that of $N_i = 20$ and 40; and (c) PDFs of local apparent order.

GCI distributions, and the probability distribution function (PDF) of the local apparent order for the regular detonation cells are also reported and plotted in Fig. 6. As shown in Fig. 6(a), the pressure curves along the centerline are nearly overlapping from the collision points. To provide a quantitative comparison, Fig. 6(b) shows the fine-GCI distributions used to assess the discretization uncertainty for individual grids. The GCI values range from 0.1 to 6.0%. Note that oscillatory convergence occurs for 47.3% of the points in the figure. The local order of accuracy p ranges from 0.01 to 13.0, with an average value of $p_{ave} = 2.16$, as shown in Fig. 6(c). The observed apparent order $p_{ave} = 2.16$ agrees with the formal order of the scheme used in this study, indicating that the grids are in the asymptotic range [37,38]. Hence, the scale $N_i = 20$ provides satisfactory precision to obtain reliable cellular detonation results and is used to solve for the propagation dynamics of detonation waves in later simulations.

IV. DISTURBED CELLS AND DISCUSSION

A. Detonation cell morphologies in a disturbed mixture

The cells of detonations longitudinally disturbed with different wavelengths λ were computed and plotted in Fig. 7. The original stable detonation, featuring very regular cells, becomes strongly unstable, and the cell features depend on λ. With a small $\lambda = 100$, in addition to the cells on the original scale, there are also new cells having scales as large as about 3 times the original cell size. These double-layer cells have been observed previously [39,40] when using special reactants, such as a nitromethane-air mixture and $H_2–N_2O$. The two-stage heat release of a nitromethane-air mixture results in a double-cellular structure. However, the mechanisms of double-layer cell formation in Fig. 7 are different. These double-layer cells are primarily due to the diverging detonation front originating from periodic decoupling and reinitiation. The small white regions in Fig. 7(a) denote
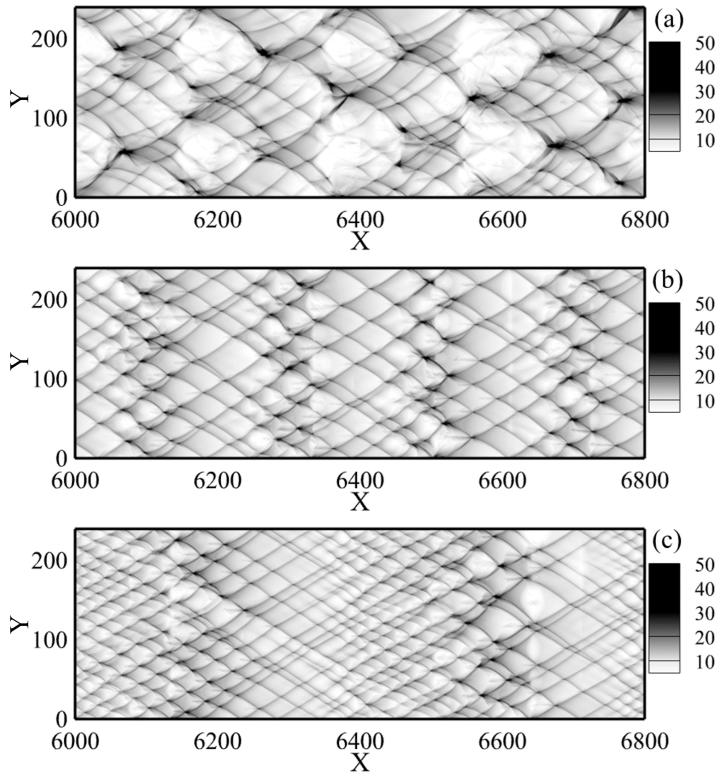
FIG. 7. Numerical cells of stable detonations with disturbance wavelength (a) $\lambda = 100$; (b) $\lambda = 200$; and (c) $\lambda = 400$.

the decoupling of the local detonation wave, and related discussion will address flow details to be displayed later.

At a moderate wavelength $\lambda = 200$, the large cell decoupled regions disappear, and the cell size mainly varies over a certain cycle. Further increasing λ to 400, the cell variation remains the same, while the disturbed cell size covers a wider range with additional small cells. The latter two cases ($\lambda = 200$ and 400) have similar cell patterns, different from the first case ($\lambda = 100$), whose cells have different length scales. The smaller wavelength combined with the regular cells for an infinite wavelength [Fig. 5(a)] results in more complex structures. The large cells are composed of some small cells, generating a double-layer cell pattern.

The averaged pressure of numerical cells is plotted in Fig. 8, with the averaging performed spatially along the vertical direction. Through this averaging, the differences between cells along the vertical direction are eliminated, leading to pressure oscillations like 1D detonations, making it convenient to compare with the results of one-dimensional pulsating detonations. The averaged pressure shows the evolution of detonation intensity along the propagation direction under the influence of a disturbance.

The density disturbance and leading shock pressure of 1D detonation are also plotted in Fig. 8 to facilitate the analysis. It is observed that the oscillation of the 2D detonation-averaged pressure has a phase shift compared with its corresponding density disturbance, and the 2D results are more irregular than 1D after averaging vertically. Phase drift is caused by mixture ignition delay and the finite-scale chemical reaction zone, resulting in a lagging response of the detonation wave to the disturbance. Whether the detonations are 1D or 2D, their pressure evolutions have shown a highly periodic oscillation following the varying disturbance. Similar phenomena have been observed in
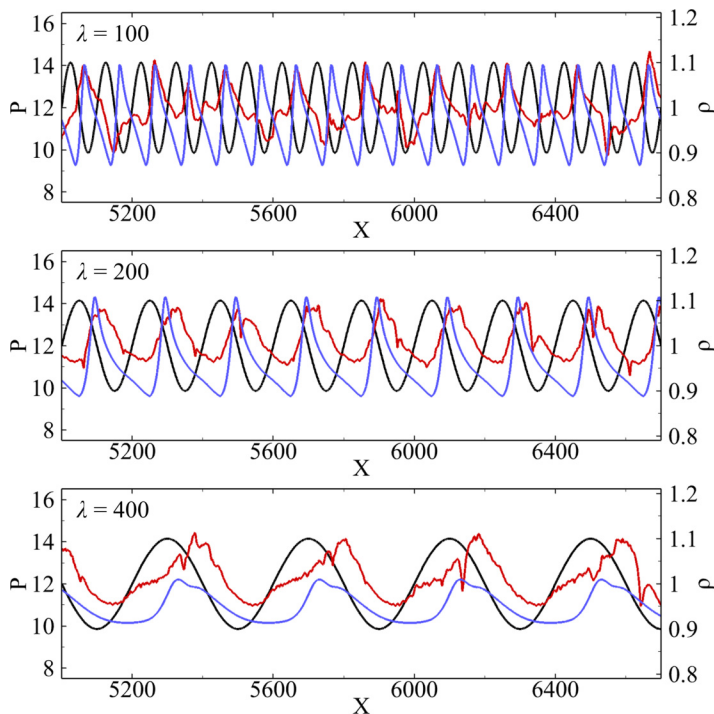
FIG. 8. Averaged cell pressure of 2D stable detonation (red), leading shock pressure of 1D detonation (blue), and sinusoidal density distribution of a nonuniform mixture (black) for different wavelengths.

a previous study [31] in which the propagation pattern is known as mode locking. The present results prove that the mode locking can happen even for 2D cellular detonations with a highly lateral instability.

But, unlike for 1D detonation, the two density cycles generate one pressure peak with very irregular profiles for the 2D detonations with a small $\lambda = 100$ in Fig. 8(a). The relationship between the averaged 2D detonation pressure and density disturbances has been obtained by calculating the power spectral density (PSD) of averaged pressure by FFT (fast Fourier transformation), as plotted in Fig. 9. The PSD can reveal the frequency characteristics of the longitudinal pressure oscillation and sinusoidal disturbance. For the three cases, the input disturbance leads to dimensionless frequencies of 0.01, 0.005, and 00025, respectively. The dominant output frequency is the same as the input frequency in the second and third cases ($\lambda = 200$ and 400, but becomes half in the first case ($\lambda = 100$). In the first case, there are also several other frequencies with nonzero PSDs, suggesting the disturbance couples with the inherent instability.

Because the averaged pressure contains no information about variations in the vertical direction, the side views of pressure with different λ are shown as line plots in Fig. 10. For infinite λ, the detonation cells in a uniform mixture have regular pressure peaks. When λ is decreased to 400, many small pressure peaks occur, becoming cluttered. Further decreasing λ induces a similar trend, and the maximum local pressure increases continuously, meaning that the transverse waves collide. For $\lambda = 100$, the maximum pressure increases to 90, nearly twice the undisturbed cell-pressure peak. The maximum pressure corresponds to the large cell, so the distances among different peaks are much larger than those in the undisturbed detonations. Many small pressure peaks are still observed, mainly from the formation of secondary triple points in the curved detonations. Hence, the double-layer cells are recorded by numerical smoke visualization, as shown in Fig. 5(a).
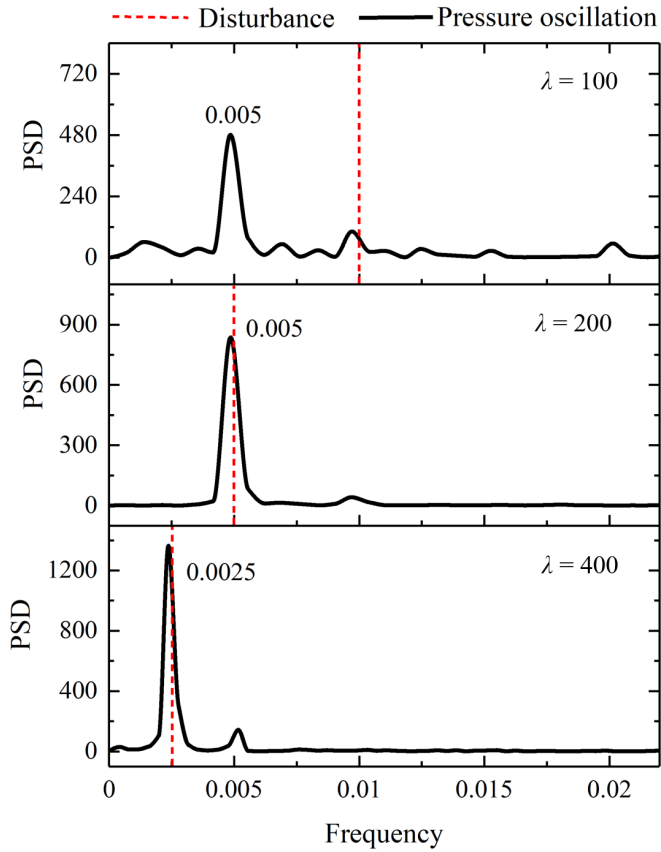
FIG. 9. Power spectral density of averaged cell pressure in stable detonations.
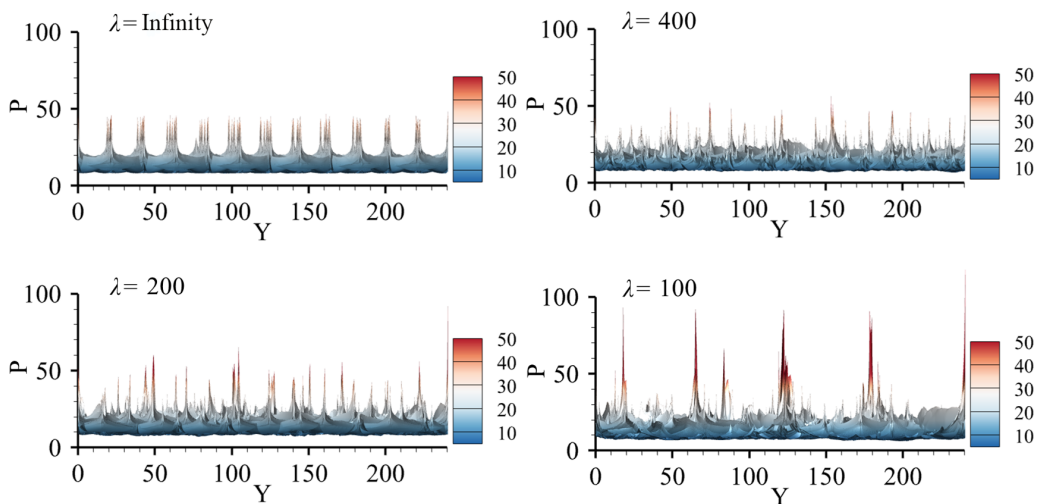

FIG. 10. Side view of pressure with different disturbance wavelengths in stable detonations.
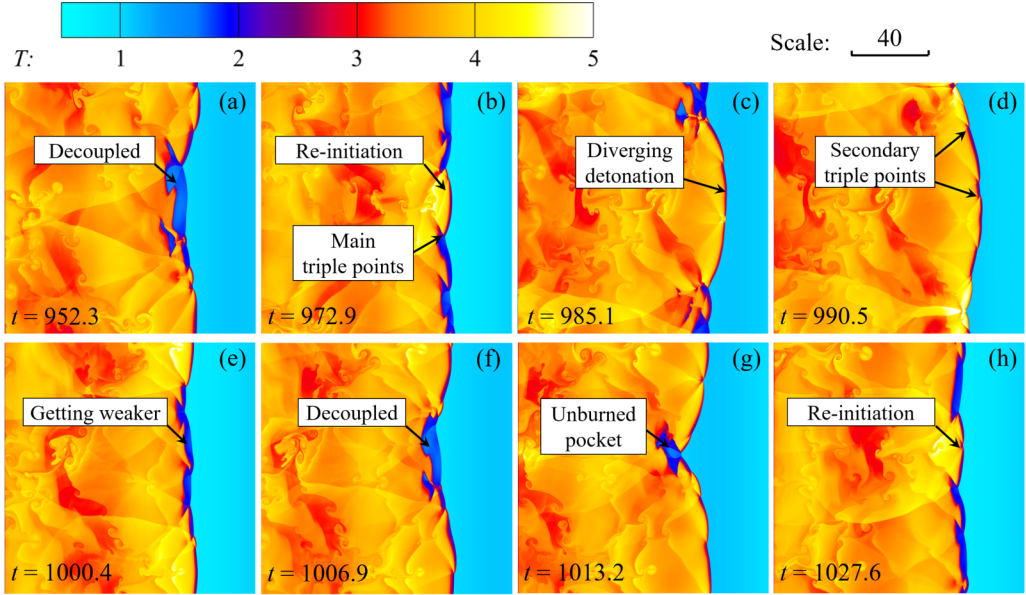
FIG. 11. Zoom-in temperature contours of the detonation wave at different instants for $T_0 = 700$ K and $\lambda = 100$.

Zoom-in temperature contours of the detonation wave at different instants are shown in Fig. 11 to analyze the formation of double-layer cell structures. As shown in Figs. 11(a) and 11(b), a pair of opposing transverse waves on either side of the incident shock collide, then the local reinitiation of the postshock mixture occurs. The newly formed Mach stem and main triple points subsequently evolve into diverging detonation. Because of the flow expansion effects of the diverging front, the curved detonation becomes weaker [see Fig. 11(e)] and has a slight decoupling on the surfaces. The decoupled and reinitiation phenomena occur periodically, leading to the formation of main triple points producing the larger cells.

The large curvature detonation wave propagates, and the flow expands to form a diverging front in Figs. 11(c) and 11(d). The middle Mach stem becomes weaker and starts to become concave. The nonuniform heat release behind the leading shock and a decrease in the overdriven degree of the detonation wave trigger kinked wave surfaces, followed by the appearance of secondary triple points on the detonation front [41], resulting in the small cells shown in Fig. 7(a). The emergence of the main and secondary triple points leads to the double-layer cell structure. This differs from the results of previous studies [39,40] in which the double-layer cells are mainly derived from a two-stage exothermic process.

By introducing the longitudinal disturbance into the unstable detonation displayed in Fig. 4, the numerical cells after long-distance propagation are plotted in Fig. 12. For small $\lambda = 100$, irregular cells are observed, and there are no obvious qualitative differences from the corresponding cells in a uniform mixture. Compared with the stable detonation case with $\lambda = 100$, local decoupling and reinitiation phenomena are not observed in Fig. 12(a). However, some separate reinitiation points [dark areas in Fig. 12(b)] arise in disturbed cells with $\lambda = 200$, forming an obscure large cell. Similar to Fig. 7(a), the Mach stem from the reinitiation point triggers a series of small cells. The double-layer cell structure appears once more but is weaker than with $\lambda = 100$ in stable detonations. Further increasing λ to 400, the large cell disappears, and only the longitudinal propagation pattern imposed by the upstream variation is observed, similar to the results for stable detonations shown in Figs. 7(b) and 7(c).
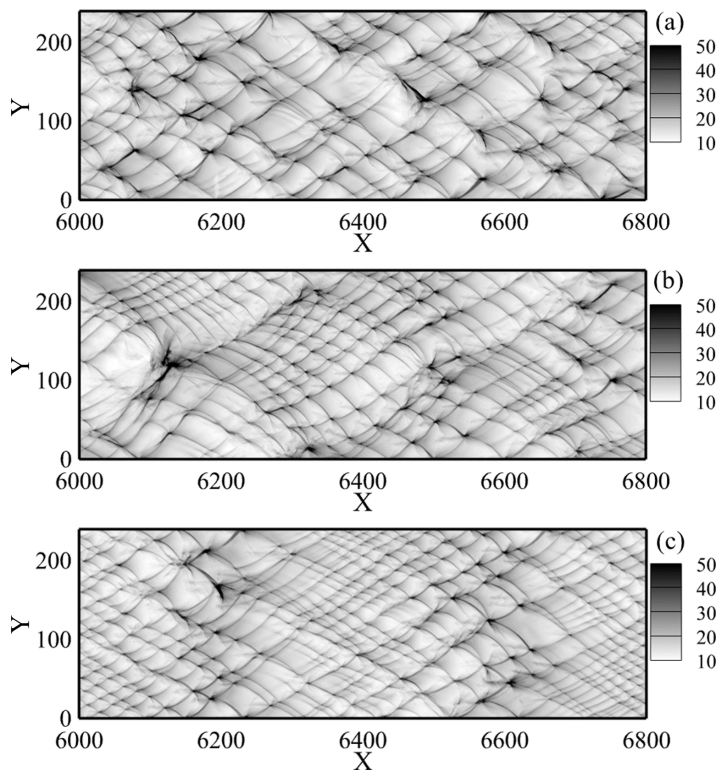
FIG. 12. Numerical cells of unstable detonations with disturbed wavelengths (a) $\lambda = 100$; (b) $\lambda = 200$; and (c) $\lambda = 400$.

Similarly, quantitative analysis has been performed by averaging the pressure of cells along the vertical direction and calculating the PSD by FFT. As shown in Fig. 13, the undisturbed detonation (infinite λ) has a wide distribution without a dominant frequency. After introducing a longitudinal disturbance, the output cell pressures always have the same dominant frequencies as the input disturbance. Comparing the three frequency distributions of disturbed cells, the large cell for $\lambda = 200$ in Fig. 13 does not induce a variation in the frequency distribution, in contrast with the last double-layer cell pattern (Fig. 9). Furthermore, the case of $\lambda = 100$ has some auxiliary frequencies that do not correspond to half or multiples of the dominant frequency. Similar phenomena can be observed in Fig. 9, demonstrating that the inherent instability plays a more important role in the case with a proper wavelength $\lambda = 100$. But, the mode-locking propagation patterns still occur over a wide disturbance wavelength, even for the highly irregular detonations.

The cell's trajectories are difficult to identify for highly irregular detonations. To describe the propagation features of detonation waves in nonuniform mixtures with different disturbance wavelengths, the propagation velocity (leftmost column), its probability distribution (center column), and PSDs of velocities (rightmost column) are shown in Fig. 14. U_{CJ} denotes the theoretical propagation speed of a steady detonation wave, and U_{ave} corresponds to the averaged velocity for a propagation distance from 3000 to 7000. From Fig. 14, the irregular detonation wave velocities fluctuate around U_{CJ}, exhibiting complex time dependence for uniform or disturbed mixtures (Fig. 14, leftmost column). The variations of disturbance wavelength slightly change the oscillation patterns but have little effect on the probability distribution of velocities (Fig. 14, center column). The velocity probability is close to a Gaussian distribution, and the related average value is observed to agree with the theoretical speed under the classical Chapman-Jouguet criterion. The PSD results reveal
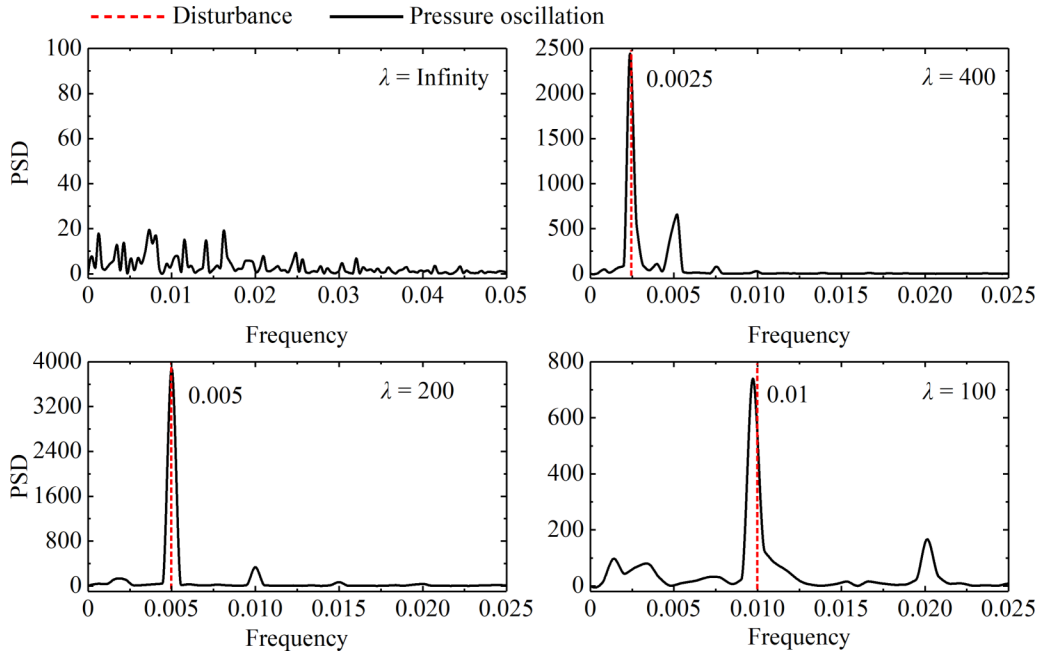
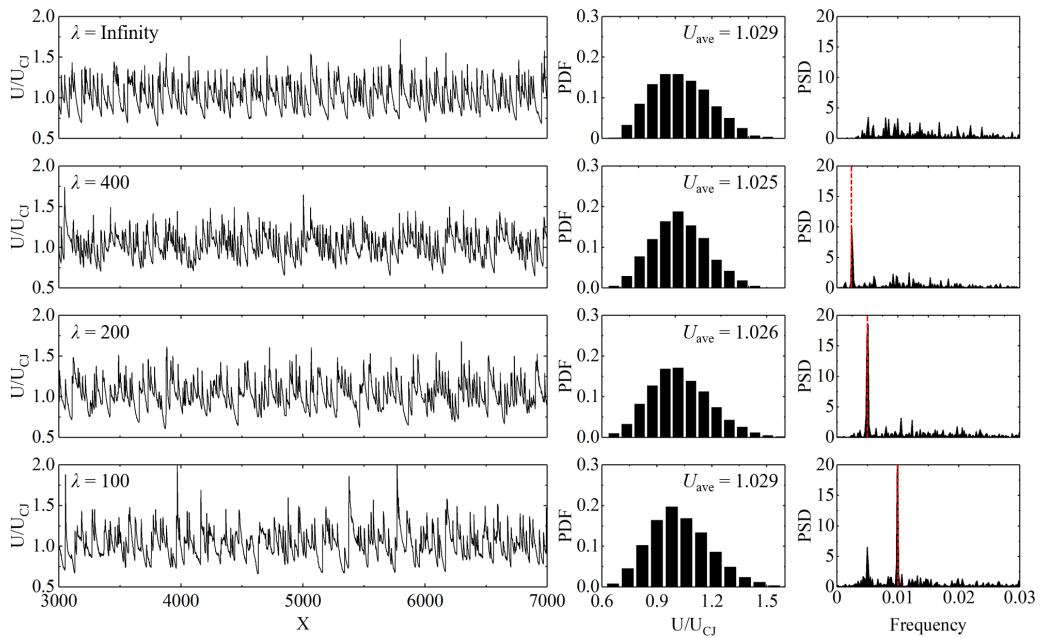FIG. 13. Power spectral density of averaged cell pressure in unstable detonations.

FIG. 14. Velocity (leftmost column), its probability distribution (center column), and PSDs of velocities (rightmost column) for unstable detonation with different disturbance wavelengths. The dashed lines in the rightmost column denote the input frequencies.
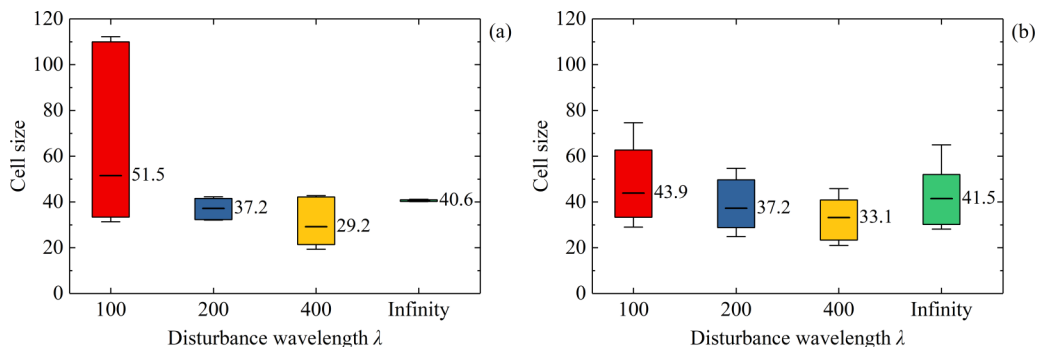
FIG. 15. Cell-size distributions of disturbed (a) stable and (b) unstable detonation.

the spectral characteristics of the velocity. The dominant frequency of the velocity oscillation is always consistent with the perturbation frequency (marked by the red dashed lines in the rightmost column), even if the perturbation wavelength is adjusted. Mode locking can also be observed in unstable detonations.

B. Discussion of the interaction of disturbance and detonation front

Cell size is a key dynamic parameter for a stable cellular detonation wave. Cell sizes change for a highly irregular detonation wave propagating in a disturbed mixture, and the features of the cell-size distribution are an important means of understanding detonation dynamics. The distribution of detonation cell sizes can be quantified using a boxplot, and the variation tendencies of cellular detonations with different disturbance wavelengths are easily identified for comparison. The cell-size distributions with varying disturbance wavelengths characterized by boxplots are shown in Fig. 15. The colored boxes represent the 90% confidence interval of the cell sizes, and the solid lines inside the boxes are the mean cell sizes. The error bars indicate maximum and minimum values, respectively. Notably, the scale of an irregular cell is defined as the vertical distance of two adjacent triple points which require the same movement direction [42]. For irregular cell structures, the triple points interfere with each other, and the movement direction is difficult to determine. Hence, the cell size of the irregular cellular front is the average distance of the two adjacent triple points.

For the stable detonations where the mixture is not disturbed, the cell size of the original detonations is almost constant (40.6), as shown in Fig. 15. The cell size is distributed in a spectrum for $\lambda = 400$, and the average size decreases to 29.2. Further decreasing λ causes the average size to increase monotonically. When λ is 100, the cell size has a wide spectrum, although the average size has increased only modestly from 40.6 to 51.5. The widest cell spectrum arises for $\lambda = 100$, which may be attributed to the formation of large cells.

For the unstable detonations, the cell size of the undisturbed detonations now has a wide spectrum. Decreasing the wavelength leads the average cell size to first decrease and then increase. The maximum averaged value appears in the case of $\lambda = 100$, identical to the stable detonations. However, the cell-size spectrum does not change drastically from the stable detonations. This is because the small cells do not disappear, even after a large cell appears when $\lambda = 200$. By contrast, the small cells disappear in some large-cell regions for $\lambda = 100$ in the stable detonations shown in Fig. 7(a), leading to a significant increase in the cell-size spectrum. Whether the small cells disappear or not depends on the evolution of the transverse waves. Generally speaking, the transverse waves are usually modest and easily weakened in stable detonations, while they are strong and resilient in unstable detonations. These transverse wave features lead to various cell-size spectrums in the disturbed detonations.
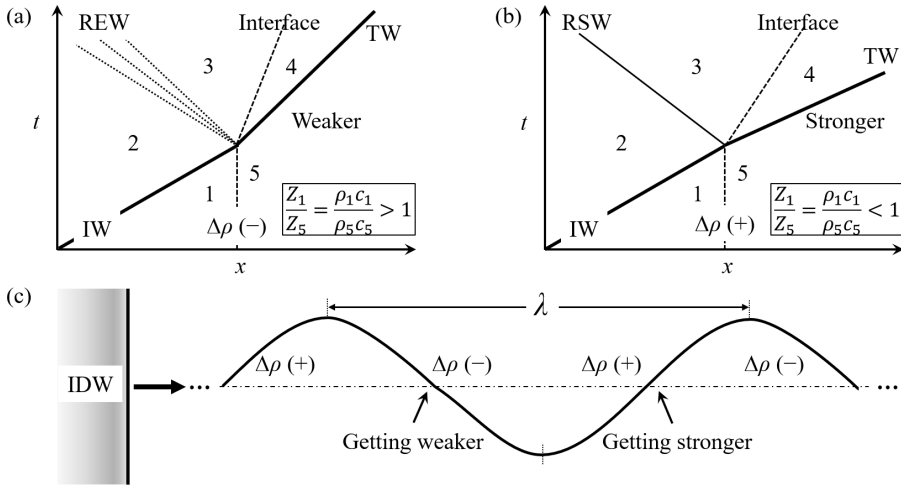
FIG. 16. The interactions of a detonation–shock wave and density interface. IW: incident wave; IDW: incident detonation wave, TW: transmitted wave, REW: reflected expansion wave, RSW: reflected shock wave.

Publications on shock-interface interaction problems typically use the acoustic impedance $Z = \rho c$ to determine the wave patterns [22,43–45], where ρ and c are the density and the speed of sound, respectively. As shown in Figs. 16(a) and 16(b), the reflected wave is an expansion wave for $Z_1/Z_5 > 1$, and the transmitted wave (TW) becomes weaker. When $Z_1/Z_5 < 1$, a reflected shock wave occurs, and the TW becomes stronger. The acoustic impedance ratio can provide a satisfactory prediction for wave patterns assuming a constant specific-heat ratio [43–45]. When a shock wave propagates in a medium with a sinusoidal density and constant pressure, the shock-wave intensity will vary periodically because of the fluctuation of the acoustic impedance ratio around unity. Similar phenomena can be observed in detonation waves in a disturbed mixture. However, more complicated wave patterns will occur for 2D cellular detonations, primarily because a detonation wave is a complex interaction of the shock and reaction fronts.

When the disturbance wavelength λ is much greater than the scale W_R of the reaction zone, the detailed reaction structures behind the leading shock wave can be neglected. Further, one incident detonation with a larger disturbance wavelength could be considered a Chapman-Jouguet wave. When a CJ detonation wave with a constant specific-heat ratio interacts with the interface, the wave patterns are similar to a nonreacting incident wave, as shown in Figs. 16(a) and 16(b). In this study, the density of the mixture varies sinusoidally, and the acoustic impedance ratio Z_1/Z_5 fluctuates near 1. The detonation wave becomes weaker for falling density and becomes stronger for rising density, as shown in Fig. 16(c). Hence, a periodic variation of cell scales is observed for a larger disturbance wavelength, as shown in Figs. 7(c) and 12(c). If the wavelength λ is close to the steady reaction-zone length scale (the dimensionless value is about 26.2 for a stable detonation and 19.1 for an unstable detonation), then the reaction-zone structures and leading shock wave are disturbed by the varying density. However, their responses to density disturbance are out of phase. The coupling relationship between leading shock and reaction zone is destroyed and rebuilt under a sinusoidal density condition.

For a stable detonation, as shown in Fig. 7(a), a density disturbance with a small wavelength λ has broken regular cells and even leads to an intermittent and local detonation decoupling. Then, the transverse waves on both sides of the decoupling region collide and trigger a local explosion. The newly formed large curvature detonation wave propagates and decays rapidly. In this process, the flow expands behind the lead shock in the presence of the diverging detonation front. The middle Mach stem part of the detonation front becomes weaker and concave after the Mach stem stretches.

Both the flame front and leading shock both converge and lead to new triple points [41]. The double-layer cell structures are observed in Fig. 7(a).

For highly irregular detonations, similar cyclical cell-size variations [Fig. 12(c)] have been observed for $\lambda \gg W_R$. When these scales have the same order of magnitude, the longitudinal disturbance will affect the coupling relationship of the reaction front and leading shock. Meanwhile, the movement of transverse waves is also strongly influenced, but their highly irregular cells are characterized by randomness and irregularity, which would offset the disturbance effects to some extent. Hence, the probability density of cell sizes under the different disturbance wavelengths exhibits no significant changes, as shown in Fig. 15(b).

V. CONCLUDING REMARKS

The propagation dynamics of cellular detonations in disturbed media have been simulated in this study. Longitudinal disturbance effects have been discussed by analyzing the numerical cells, pressures, and velocities of the detonation waves.

The results indicate that numerical smoke-cell scales vary with an approximate single-mode oscillation for larger disturbance wavelengths. It is observed that upstream density variations impose the periodic oscillations of the average leading shock pressure. This observation means that when the longitudinal disturbance wavelength is much greater than the reaction-zone width, mode locking of detonation dynamics still occurs in cellular detonations both for regular and irregular detonations.

The acoustic impedance used to determine the wave patterns is introduced to analyze detonation-interface interactions to clarify this point. For regular detonations, if the disturbance wavelength is close to the steady reaction-zone length scale, the density disturbance could trigger a vertical instability, resulting in local reinitiation of the decoupling detonation wave. Therefore, large cells whose size reaches about 3–6 times the original cell size are observed, leading to a double-layer cell pattern. However, there are different cell sizes and velocity spectra in regular and irregular detonations that can be attributed to different features of transverse waves and their roles in cell evolution.

ACKNOWLEDGMENTS

---

[1] W. Fickett and W. Davis, *Detonation: Theory and Experiment* (Dover, New York, 1979).

[2] H. D. Ng, Y. Ju, and J. H. S. Lee, Assessment of detonation hazards in high-pressure hydrogen storage from chemical sensitivity analysis, Int. J. Hydrogen Energ. **32**, 93 (2007).

[3] J. H. S. Lee, *The Detonation Phenomenon* (Cambridge University Press, Cambridge, 2008).

[4] K. Kailasanath, Review of propulsion applications of detonation waves, AIAA J. **38**, 1698 (2000).

[5] J. Chan, J. P. Sislian, and D. Alexander, Numerically simulated comparative performance of a Scramjet and Shcramjet at Mach 11, J. Propuls. Power **26**, 1125 (2010).

[6] V. Anand and E. Gutmark, Rotating detonation combustors and their similarities to rocket instabilities, Prog. Energ. Combust. **73**, 182 (2019).

[7] H. Teng, Y. Zhang, P. Yang, and Z. Jiang, Oblique detonation wave triggered by a double wedge in hypersonic flow, Chin. J. Aeronaut **35**, 176 (2022).

[8] J. Urzay, Supersonic combustion in air-breathing propulsion systems for hypersonic flight, Annu. Rev. Fluid Mech. **50**, 593 (2018).

[9] Z. Jiang, Z. Zhang, Y. Liu, C. Wang, and C. Luo, The criteria for hypersonic airbreathing propulsion and its experimental verification, Chin. J. Aeronaut **34**, 94 (2021).

[10] M. Zhao, M. J. Cleary, and H. Zhang, Combustion mode and wave multiplicity in rotating detonative combustion with separate reactant injection, Combust. Flame **225**, 291 (2021).

[11] C. Yan, H. Teng, and H. D. Ng, Effects of slot injection on detonation wavelet characteristics in a rotating detonation engine, Acta. Astronaut **182**, 274 (2021).

[12] P. Yang, H. D. Ng, and H. Teng, Unsteady dynamics of wedge-induced oblique detonations under periodic inflows, Phys. Fluids **33**, 016107 (2021).

[13] X. Guo, Z. Zhai, T. Si, and X. Luo, Bubble merger in initial Richtmyer-Meshkov instability on inverse-chevron interface, Phys. Rev. Fluids **4**, 092001(R) (2019).

[14] S. Hemchandra, S. Shanbhogue, S. Hong, and A. F. Ghoniem, Role of hydrodynamic shear layer stability in driving combustion instability in a premixed propane-air backward-facing step combustor, Phys. Rev. Fluids **3**, 063201 (2018).

[15] Z. Pan, K. Chen, J. Qi, P. Zhang, Y. Zhu, J. Pan, and M. Gui, The propagation characteristics of curved detonation wave: Experiments in helical channels, Proc. Combust. Inst. **37**, 3585 (2019).

[16] X. Mi, A. Higgins, C. Kiyanda, H. D. Ng, and N. Nikiforakis, Effect of spatial inhomogeneities on detonation propagation with yielding confinement, Shock Waves **28**, 993 (2018).

[17] K. Ishii and M. Kojima, Behavior of detonation propagation in mixtures with concentration gradients, Shock Waves **17**, 95 (2007).

[18] D. A. Kessler, V. N. Gamezo, and E. S. Oran, Gas-phase detonation propagation in mixture composition gradients, Philos. Trans. R. Soc. A. **37**, 567 (2012).

[19] L. R. Boeck, F. M. Berger, J. Hasslberger, and T. Sattelmayer, Detonation propagation in hydrogen-air mixtures with transverse concentration gradients, Shock Waves **26**, 181 (2016).

[20] S. Boulal, P. Vidal, and R. Zitoun, Experimental investigation of detonation quenching in non-uniform compositions, Combust. Flame **172**, 222 (2016).

[21] S. Boulal, P. Vidal, R. Zitoun, T. Matsumoto, and A. Matsuo, Experimental investigation on detonation dynamics through a reactivity sink, Combust. Flame **196**, 11 (2018).

[22] K. C. Tang Yuk, X. C. Mi, J. H. S. Lee, and H. D. Ng, Transmission of a detonation across a density interface, Shock Waves **28**, 967 (2018).

[23] K. C. Tang Yuk, X. C. Mi, J. H. S. Lee, H. D. Ng, and R. Deiterding, Transmission of a detonation wave across an inert layer, Combust. Flame **236**, 111769 (2022).

[24] Y. Wang, C. Huang, R. Deiterding, H. Chen, and Z. Chen, Propagation of gaseous detonation across inert layers, Proc. Combust. Inst. **38**, 3555 (2021).

[25] X. Mi, E. V. Timofeev, and A. Higgins, Effect of spatial discretization of energy on detonation wave propagation, J. Fluid Mech. **817**, 306 (2017).

[26] X. Mi, A. Higgins, H. D. Ng, C. Kiyanda, and N. Nikiforakis, Propagation of gaseous detonation waves in a spatially inhomogeneous reactive medium, Phys. Rev. Fluids **2**, 053201 (2017).

[27] D. A. Rosato, M. Thornton, J. Reyes, and K. A. Ahmed, Fuel distribution measurements in a hypersonic combustor facility, in *Proceedings of the AIAA Propulsion and Energy 2021 Forum* (AIAA, 2021), paper 3526.

[28] D. A. Rosato, M. Thornton, J. Sosa, C. Bachman, G. B. Goodwin, and K. A. Ahmed, Stabilized detonation for hypersonic propulsion, Proc. Natl. Acad. Sci. USA **118**, e2102244118 (2021).

[29] W. Ma, C. Wang, and W. Han, Effect of concentration inhomogeneity on the pulsating instability of hydrogen-oxygen detonations, Shock Waves **30**, 703 (2020).

[30] M. Kim, X. Mi, C. Kiyanda, and H. D. Ng, Nonlinear dynamics and chaos regularization of one-dimensional pulsating detonations with small sinusoidal density perturbations, Proc. Combust. Inst. **38**, 3701 (2021).

[31] A. R. Kasimov and A. R. Gonchar, Reactive Burgers model for detonation propagation in a non-uniform medium, Proc. Combust. Inst. **38**, 3725 (2021).

[32] K. Mazaheri, Y. Mahmoudi, and M. I. Radulescu, Diffusion and hydrodynamic instabilities in gaseous detonations, Combust. Flame **159**, 2138 (2012).

[33] H. D. Ng, M. I. Radulescu, A. Higgins, N. Nikiforakis, and J. H. S. Lee, Numerical investigation of the instability for one-dimensional Chapman-Jouguet detonations with chain-branching kinetics, Combust. Theor. Model **9**, 385 (2005).

[34] H. Teng, L. Zhou, P. Yang, and Z. Jiang, Numerical investigation of wavelet features in rotating detonations with a two-step induction-reaction model, Int. J. Hydrogen Energ. **45**, 4991 (2020).

[35] M. I. Radulescu and B. M. Maxwell, The mechanism of detonation attenuation by a porous medium and its subsequent re-initiation, J. Fluid Mech. **667**, 96 (2011).

[36] K. H. Kim, C. Kim, and O. H. Rho, Methods for the accurate computations of hypersonic flows I. AUSMPW+ scheme, J. Comput. Phys. **174**, 38 (2001).

[37] I. Celik and O. Karatekin, Numerical experiments on application of Richardson extrapolation with nonuniform grids, ASME. J. Fluids Eng. **584**, 119 (1997).

[38] I. B. Celik, U. Ghia, P. J. Roache, C. J. Freitas, H. Coleman, and P. E. Raad, Procedure for estimation and reporting of uncertainty due to discretization in CFD applications, ASME. J. Fluids Eng. **130**, 078001 (2008).

[39] H. D. Ng and F. Zhang, Detonation instability, in *Shock Waves Science and Technology Library*, edited by F. Zhang (Springer, Berlin, Heidelberg, 2012), Vol. 6.

[40] Y. Sugiyama and A. Matsuo, On the characteristics of two-dimensional double cellular detonations with two successive reactions model, Proc. Combust. Inst. **33**, 2227 (2011).

[41] Z. Jiang, G. Han, C. Wang, and F. Zhang, Self-organized generation of transverse waves in diverging cylindrical detonations, Combust. Flame **156**, 1653 (2009).

[42] G. J. Sharpe and M. I. Radulescu, Statistical analysis of cellular detonation dynamics from numerical simulations: One-step chemistry, Combust. Theor. Model **15**, 691 (2011).

[43] J. H. J. Niederhaus, J. A. Greenough, J. G. Oakley, D. Ranjan, M. H. Anderson, and R. Bonazza, A computational parameter study for the three-dimensional shock–bubble interaction, J. Fluid Mech. **594**, 85 (2008).

[44] D. Ranjan, J. Oakley, and R. Bonazza, Shock-bubble interactions, Annu. Rev. Fluid Mech. **43**, 117 (2011).

[45] A. Haselbacher, On impedance in shock-refraction problems, Shock Waves **22**, 381 (2012).